Research Article | Vol. 27, No. 9 | 29 Apr 2019 | OPTICS EXPRESS 11979
Optics EXPRESS

Modelling spontaneous four-wave mixing in periodically tapered waveguides

MOHAMMED F. SALEH[1,2,*]

[1]Scottish Universities Physics Alliance (SUPA), Institute of Photonics and Quantum Sciences, Heriot-Watt University, EH14 4AS Edinburgh, United Kingdom
[2]Department of Mathematics and Engineering Physics, Alexandria University, Alexandria, Egypt
[*]m.saleh@hw.ac.uk

Abstract: A periodically tapered waveguides technique is an emerging potential route to establish quasi-phase-matching schemes in third-order nonlinear materials for efficient on-demand parametric interactions. In this paper, I investigate this method in enhancing spontaneous photon-pair emission in microstructured fibres and planar waveguides with sinusoidally varying cross sections. To study this process for continuous and pulsed-pump excitations, I have developed a general robust quantum model that takes into account self- and cross-phase modulations. The model shows a great enhancement in photon-pair generation in waveguides with a small number of tapering periods that are feasible via the current fabrication technologies. I envisage that this work will open a new area of research to investigate how the tapering patterns can be fully optimised to tailor the spectral properties of the output photons in nonlinear guided structures.

1. Introduction

Spontaneous photon-pair emission in nonlinear media has become the standard approach for preparing quantum states of light in labs due to its efficiency, ease of use, and operation at practical conditions [1]. In second-order nonlinear media, a mother photon can be downconverted into two daughter photons in three-wave mixing process. Whereas, two pump photons will combine to generate two other photons in a spontaneous four-wave mixing (SFWM) parametric interaction in third-order nonlinear media.

Efficient parametric wave-mixing processes are inherently constrained by energy and momentum conservation (the latter is known as the phase-matching condition). Quasi-phase-matching schemes have been successfully employed in second-order nonlinear media to enable on-demand parametric processes, using periodically poled ferroelectric crystals [2, 3]. This technique has had a remarkable impact in the field of nonlinear and quantum optics; it eliminates the stringent constraints posed on the directions and polarisations of the interacting waves, and allows for on-chip collinear co-polarised strong nonlinear interactions to take place. Using this technique, highly efficient and pure single-photon sources have been widely demonstrated in bulk and integrated configurations [4–6].

Silica fibres and silicon-photonic waveguides are the practical and convenient platforms for generating single photons for quantum networking and integrated-quantum applications, respectively [7, 8]. Enabling SFWM parametric processes in these third-order nonlinear platforms can be achieved via exploiting the nearly phase-matching regime, or balancing waveguide and material dispersions [9]. Similar to second-order nonlinear media, these conventional methods poses restrictions, for instance, the frequency-separation between the interacting photons and the operating dispersion regime. Other alternative techniques such as photonic crystal fibres [10, 11], birefringent silica waveguides [1, 5], microresonantors [12], symmetric and asymmetric directional couplers [13, 14] have shown the ability to circumvent these limitations to obtain highly efficient and pure single photons in third-order nonlinear media.

In analogue to periodically poled structures, periodically tapered waveguides (PTWs) have been

#358178 https://doi.org/10.1364/OE.27.011979
Journal © 2019 Received 21 Jan 2019; revised 29 Mar 2019; accepted 29 Mar 2019; published 15 Apr 2019

Optics EXPRESS

also introduced to correct phase mismatching of third-order nonlinear interactions via sinusoidally modulating the width of planar waveguides or the core of microstructured fibres (coined as dispersion-oscillating fibres) along the propagation direction [15–17]. The tapering period was initially restricted to the millimetre range in planar structures. Very recently, PTWs with tapering periods in the micrometer range have been successfully realised in planar waveguides in two different configurations with either modulating the core or the cladding using the Photonic Damascene process [18]. These structures have been mainly exploited in tuning dispersive-wave emission, controlling supercontinuum generation, and manipulating modulation instability. On the theoretical side, I have presented a new analysis based on the Fourier-series to explain how PTWs can be employed as a complete analogue to periodically poled structures [19]. In PTWs both the linear and nonlinear coefficients are longitudinally varying resulting in multiple Fourier components of the phase-mismatching and nonlinear terms. Opposite Fourier components of the two terms can simultaneously cancel each other, if right combinations of the tapering period and modulation amplitude of the waveguide are used, allowing the conversion efficiency of a parametric process to grow along the structure.

In this paper, I have applied the PTW-technique to generate photon pairs via SFWM processes at on-demand frequencies and with relatively high spectral purity. The paper is organised as follows. In Sec. 2, a robust quantum model have been developed to study this process in tapered waveguides for continuous and pulsed pump sources. This model has then been applied to study SFWM processes in dispersion-oscillating fibres and width-modulated planar silicon-nitride waveguides in Sec. 3. Finally, my conclusions are summarised in Sec. 4.

2. Modelling SFWMs processes in PTWs

Consider a SFWM parametric process in a single-mode third-order nonlinear waveguide. I have developed a model in the Heisenberg picture following an approach that determines the energy flux across a transverse plane inside the waveguide over a long quantisation time T [20]. The Hamiltonian in this approach is determined by calculating the number of photons that cross this plane at a certain frequency multiplied by the corresponding energy of each photon, then summing over all the possible frequencies. Initially, it is assumed that the pump is a monochromatic wave and the waveguide has a longitudinally uniform cross-section. Later, the model will be generalised to take into account propagation in tapered waveguides, as well as having pulsed pump sources. If the common interaction Hamiltonian model [21] were to apply for this problem, one will immediately run in a trouble since the refractive index becomes spatial-dependent in tapered waveguides. However, the developed theoretical framework circumvents this problem. Raman nonlinearity is neglected, for simplicity, which is also the case in silicon-nitride waveguides [22] and hollow-core fibres filled by noble gases [23]. Moreover, its influence can be minimised by generating photon pairs far from the Raman gain peak using the PTW-technique [16].

2.1. Continuous pump wave

Assuming that the pump (p) is a strong undepleted monochromatic classical wave, its electric field can be described as

$$\mathcal{E}_p(x,y,z,t) = \mathbf{Re}\left\{E_p(x,y,z,t)\right\}, \tag{1}$$

where x, y are the transverse coordinates, z is the longitudinal direction, t is the time, **Re** is the real part, $E_p = A_p F_p(x,y)\, e^{-j(\omega_p t - k_p z)}$, A_p, F_p, ω_p, k_p are the amplitude, transverse profile, angular frequency, and propagation constant of the pump wave, respectively, $k_p = n_p\omega_p/c$, n_p is the refractive index at the pump frequency, and c is the speed of light in vacuum. Using Maxwell equations and applying the slowly varying approximation [9], the self-phase modulation effect

Optics EXPRESS

that influences the pump propagation can be included by replacing k_p with

$$\kappa_p = k_p \left[1 + \frac{3\chi^{(3)} A_p^2}{8\, n_p^2\, S_p} \iint \left| F_p \right|^4 dxdy \right], \tag{2}$$

where $\chi^{(3)}$ is the nonlinear coefficient, and $S_p = \iint \left| F_p \right|^2 dxdy$ is the pump beam area.

2.2. Signal and idler photons

The electric field operators of the converted single photons (either signal or idler) can be written as

$$\hat{\mathcal{E}}\left(x, y, z, t\right) = \hat{\mathcal{E}}^{+}\left(x, y, z, t\right) + \hat{\mathcal{E}}^{-}\left(x, y, z, t\right), \tag{3}$$

where $\hat{\mathcal{E}}^{+}$ and $\hat{\mathcal{E}}^{-}$ are the positive and negative frequency-components of the field, $\hat{\mathcal{E}}^{-} = \left(\hat{\mathcal{E}}^{+}\right)^{\dagger}$, and $\hat{\mathcal{E}}^{+}$ can be expressed in terms of a superposition of frequency-dependent mode operators [20],

$$\hat{\mathcal{E}}^{+}\left(x, y, z, t\right) = \sum_{s} \sqrt{\frac{\hbar\omega_s}{2\epsilon_o c T n_s S_s}} F_s\left(x, y\right) \hat{a}\left(z, \omega_s\right) e^{-j\omega_s t}, \tag{4}$$

F, S, ω, and n have the same definitions as for the pump wave, $\hbar$ is the reduced Planck's constant, ϵ_o is the dielectric permittivity, and $\hat{a}$ is annihilation operator. The discrete spectral modes are separated by a frequency spacing $2\pi/T$, where T approaches ∞. The photon-number operator of mode s during a time window T is $\hat{N}\left(z, \omega_s\right) = \hat{a}^{\dagger}\left(z, \omega_s\right) \hat{a}\left(z, \omega_s\right)$ with $\hat{a}^{\dagger}$ the creation operator. The space evolution of the operators are governed by [20, 24]

$$-j\hbar \frac{\partial \hat{\mathcal{E}}}{\partial z} = \left[\hat{\mathcal{E}}, \hat{G}\right], \tag{5}$$

where $\hat{G}\left(z\right) = \iint \int_0^T \hat{g}\left(x, y, z, t\right) dt\, dxdy$ is the momentum operator, $\hat{g} = \hat{\mathcal{D}}^{+}\hat{\mathcal{E}}^{-} + \text{H.c.}$ is the momentum-flux operator, $\hat{\mathcal{D}} = \epsilon_o n^2 \hat{\mathcal{E}} + \hat{\mathcal{P}}_{\text{NL}}$ is the electric-displacement field operator, $\hat{\mathcal{P}}_{\text{NL}}$ is the nonlinear-polarisation operator , and H.c. is the Hermitian conjugate.

2.3. Linear propagation

Via substituting in Eq. (5) the electric-field and momentum operators by their definitions, it can be easily shown in the linear regime (L) that

$$\frac{\partial \hat{a}_s^{(\text{L})}}{\partial z} = j k_s \hat{a}_s\left(z\right), \tag{6}$$

where the commutation relation $\left[\hat{a}\left(z, \omega_s\right), \hat{a}^{\dagger}\left(z, \omega_{s'}\right)\right] = \delta_{ss'}$ has been applied, with δ a Kroenecker delta, $k_s = n_s\omega_s/c$, and $\hat{a}_s\left(z\right) = \hat{a}\left(z, \omega_s\right)$ for brevity.

2.4. Spontaneous four-wave mixing process

To study a SFWM interaction in this picture, the positive frequency-part of the nonlinear polarisation operator associated with this process should be first determined, $\hat{\mathcal{P}}^{+}_{\text{FWM}} = 3\epsilon_o \chi^{(3)} E_p E_p \hat{\mathcal{E}}^{-}$. The momentum-flux operator is then given by $\hat{g}_{\text{FWM}} = \hat{\mathcal{P}}^{+}_{\text{FWM}} \hat{\mathcal{E}}^{-} + \text{H.c.}$ Applying the definition of the delta function $\delta\left(\Delta\omega\right) = \frac{1}{T}\int_0^T \exp\left(-j\Delta\omega t\right) dt$, the momentum operator in this case is determined as

$$\hat{G}_{\text{FWM}} = \frac{3\hbar\chi^{(3)} A_p^2 e^{j2\kappa_p z}}{8c} \sum_{s} \sqrt{\frac{\omega_s\omega_i}{n_s n_i S_s S_i}} \iint F_p^2 F_s^* F_i^*\, dxdy\; \hat{a}_s^{\dagger}\left(z\right) \hat{a}_i^{\dagger}\left(z\right) + \text{H.c.}, \tag{7}$$

Optics EXPRESS

with $\omega_i = 2\omega_p - \omega_s$. The subscript i refers to another mode that is coupled to the mode s within the spectrum of the output photons. Substituting $\hat{G}_{\mathrm{FWM}}$ in Eq. (5), the space evolution of the mode operator s due to this process is

$$\frac{\partial \hat{a}_s^{(\mathrm{FWM})}}{\partial z} = j\frac{3\chi^{(3)}A_p^2 e^{j2\kappa_p z}}{4c}\sqrt{\frac{\omega_s\omega_i}{n_s n_i S_s S_i}}\iint F_p^2 F_s^* F_i^* dxdy \;\; \hat{a}_i^\dagger(z). \tag{8}$$

2.5. Cross-phase modulation (XPM) effect

Following the aforementioned procedure, the nonlinear part of the momentum-flux operator due to the XPM effect is given by $\hat{g}_{\mathrm{XPM}} = 6\epsilon_o\chi^{(3)}E_p E_p^*\hat{\mathcal{E}}^+\hat{\mathcal{E}}^- + \mathrm{H.c}$. Hence, the momentum operator of this effect is

$$\hat{G}_{\mathrm{XPM}} = \frac{3\hbar\chi^{(3)}A_p^2}{4c}\sum_s \frac{\omega_s}{n_s S_s}\iint |F_p|^2 |F_s|^2 dxdy\; \hat{a}_s(z)\hat{a}_s^\dagger(z) + \mathrm{H.c.}, \tag{9}$$

and the annihilation operator is spatially evolved as

$$\frac{\partial \hat{a}_s^{(\mathrm{XPM})}}{\partial z} = j\frac{3\chi^{(3)}A_p^2}{2c}\frac{\omega_s}{n_s S_s}\iint |F_p|^2 |F_s|^2 dxdy \;\; \hat{a}_s(z). \tag{10}$$

2.6. Total effects

Therefore, the evolution of the mode operator s due to linear and nonlinear contributions can be written as

$$\frac{\partial \hat{a}_s}{\partial z} = \frac{\partial \hat{a}_s^{(\mathrm{L})}}{\partial z} + \frac{\partial \hat{a}_s^{(\mathrm{XPM})}}{\partial z} + \frac{\partial \hat{a}_s^{(\mathrm{FWM})}}{\partial z} = j\kappa_s\hat{a}_s(z) + j\gamma_{s,i}\, e^{j2\kappa_p z}\hat{a}_i^\dagger(z), \tag{11}$$

with

$$\kappa_s = k_s\left(1 + \frac{3\chi^{(3)}A_p^2}{2n_s^2 S_s}\iint |F_p|^2 |F_s|^2 dxdy\right), \tag{12}$$

and

$$\gamma_{s,i} = \frac{3\chi^{(3)}A_p^2}{4c}\sqrt{\frac{\omega_s\omega_i}{n_s n_i S_s S_i}}\iint F_p^2 F_s^* F_i^* dxdy. \tag{13}$$

A similar equation can be written for the creation operator of the mode i,

$$\frac{\partial \hat{a}_i^\dagger}{\partial z} = -j\kappa_i^*\hat{a}_i^\dagger(z) - j\gamma_{s,i}^*\, e^{-j2\kappa_p z}\hat{a}_s(z). \tag{14}$$

The two coupled Eqs. (11) and (14) can be solved exactly in the case of uniform waveguides, similar to the spontaneous parametric downconversion process [20].

2.7. Transfer matrix method

Introducing the phase transformation $\hat{a}_q(z) = \hat{b}_q(z)\;\; e^{j\kappa_q z}$, $q = s, i$, Eqs. (11) and (14) can be written in the common compact form,

$$\frac{\partial \hat{b}_s}{\partial z} = j\gamma_{s,i}\, e^{j\Delta\kappa z}\hat{b}_i^\dagger(z), \qquad \frac{\partial \hat{b}_i^\dagger}{\partial z} = -j\gamma_{s,i}^*\, e^{-j\Delta\kappa z}\hat{b}_s(z), \tag{15}$$

with $\Delta\kappa = 2\kappa_p - \kappa_s - \kappa_i$. If the waveguide is tapered, the coefficients in these equations become spatial dependent. Also, the term $e^{j\Delta\kappa z}$ should be replaced by $e^{j\Delta\phi}$, with $\Delta\phi = \int_0^z \Delta\kappa(z')\, z'\, dz'$

the proper accumulated phase-mismatching [3,25]. To solve the coupled equations in this case, the waveguide can be truncated into discrete infinitesimal elements with constant cross sections, then these equations can be solved within each element. The outcome of an element m can be written in a transfer-matrix form,

$$\begin{bmatrix} \hat{b}_s \\ \hat{b}_i^\dagger \end{bmatrix}_{z=z_m+\Delta z} = \mathcal{T}_m \begin{bmatrix} \hat{b}_s \\ \hat{b}_i^\dagger \end{bmatrix}_{z=z_m}, \qquad \mathcal{T}_m = \begin{bmatrix} 1 & f_{s,i}\left(\omega_p\right) \\ f_{s,i}^*\left(\omega_p\right) & 1 \end{bmatrix}_{z=z_m}, \tag{16}$$

with $f_{s,i}\left(\omega_p\right) = j\gamma_{s,i}\Delta z\, e^{j\Delta\phi}$ and Δz the element thickness. The explicit dependence of the parameter $f_{s,i}$ on ω_p has been shown here, to remind the reader that all these matrix elements depend on the pump frequency. The transfer matrix that describes the whole structure and relates the output operators to the input ones is given by the multiplication of the transfer matrices of all elements in a descending order, $\mathbf{T}_{s,i} = \mathcal{T}_M\mathcal{T}_{M-1}...\mathcal{T}_2\mathcal{T}_1$, with M the elements number. It is worth to note that each element has a different transfer matrix even in periodic structures, because of the parameter $\Delta\phi$ that always counts the accumulated phase from the beginning of the structure.

2.8. Expected number of photons

The expected number of photons of a certain mode s at the end of the waveguide is given by $\langle\psi|\,\hat{N}\left(L,\omega_s\right)|\psi\rangle = \langle\psi|\,\hat{b}_s^\dagger\left(L\right)\hat{b}_s\left(L\right)|\psi\rangle$, with $|\psi\rangle = |0\rangle_s\,|0\rangle_i$ the input quantum state and L the waveguide length. Using the transfer matrix of the whole structure, $\hat{b}_s\left(L\right) = \mathbf{T}_{s,i}\left(1,1\right)\hat{b}_s\left(0\right) + \mathbf{T}_{s,i}\left(1,2\right)\hat{b}_i^\dagger\left(0\right)$, subsequently $\langle\psi|\,\hat{N}\left(L,\omega_s\right)|\psi\rangle = \left|\mathbf{T}_{s,i}\left(1,2\right)\right|^2$. It is important to mention that this procedure is only for a single mode s and it should be repeated for all other modes that compose the signal spectrum.

2.9. Pulsed pump source

The model that I have developed so far is based on having a monochromatic pump source. If the pump is assumed to be a Gaussian pulse with a characteristic temporal width τ and a central frequency ω_{p_0}, then $E_p = \mathcal{A}\left(t\right)F_p\left(x,y\right)e^{jk_pz}$, where $\mathcal{A}\left(t\right) = A_0e^{-t^2/2\tau^2}e^{-j\omega_{p_0}t}$ is the pulse temporal dependence and the full-width-half-maximum of this pulse equals $2\tau\sqrt{\ln(2)}$. Using the Fourier Transform, the pump electric field can be decomposed into a superposition of multiple monochromatic waves with frequencies ω_p,

$$\mathcal{E}_p\left(x,y,z,t\right) = \mathbf{Re}\left\{\sum_{\omega_p} A_p\left(\omega_p\right)\, e^{-j\left(\omega_p t - k_p z\right)}\right\}, \tag{17}$$

where $A_p\left(\omega_p\right) = \frac{A_0\tau\Delta\omega}{\sqrt{2\pi}}\, e^{-\frac{\tau^2\left(\omega_p-\omega_{p_0}\right)^2}{2}}$ is the amplitude of each component, and $\Delta\omega$ is the sample frequency of the pump pulse.

To study how the evolution of two certain coupled modes s and i in the signal spectrum is influenced by having a pulsed-pump source, each possible combination of two monochromatic waves ω_{p_1} and ω_{p_2} within the pump spectrum should be counted towards the evolution of these modes. Because of the energy conservation or the delta function used in defining the momentum operator $\hat{G}_{\mathrm{FWM}}$, the double summation over ω_{p_1} and ω_{p_2} is reduced to a single summation over ω_{p_1} with $\omega_{p_2} = \omega_s + \omega_i - \omega_{p_1}$. The above procedure to determine the expected number of photons can still be followed, however, the transfer matrix of an element m in this case becomes

$$\mathcal{T}_m = \begin{bmatrix} 1 & \sum\limits_{\omega_{p_1}} f_{s,i}\left(\omega_{p_1},\omega_{p_2}\right) \\ \sum\limits_{\omega_{p_1}} f_{s,i}^*\left(\omega_{p_1},\omega_{p_2}\right) & 1 \end{bmatrix}_{z=z_u}. \tag{18}$$

Optics EXPRESS

For *non-degenerate* combinations of ω_{p_1} and ω_{p_2},

$$\gamma_{s,i} = \frac{3\chi^{(3)} A_{p_1} A_{p_2}}{2c} \sqrt{\frac{\omega_s \omega_i}{n_s n_i S_s S_i}} \iint F_{p_1} F_{p_2} F_s^* F_i^* \, dxdy, \tag{19}$$

and $\Delta\kappa = \kappa_{p_1} + \kappa_{p_2} - \kappa_s - \kappa_i$. Also, each monochromatic pump wave in this case will induce a XPM effect that will influence the other pump wave as well as the converted single photons. Therefore,

$$\kappa_{p_u} = k_{p_u} \left[1 + \frac{3\chi^{(3)}}{8\, n_{p_u}^2 S_{p_u}} \iint \left(A_{p_u}^2 \left|F_{p_u}\right|^2 + 2A_{p_v}^2 \left|F_{p_v}\right|^2 \right) \left|F_{p_u}\right|^2 dxdy \right], \quad \begin{cases} u, v = 1, 2 \\ u \neq v \end{cases}, \tag{20}$$

and

$$\kappa_q = k_q \left[1 + \frac{3\chi^{(3)}}{2n_q^2 S_q} \iint \left(A_{p_1}^2 \left|F_{p_1}\right|^2 + A_{p_2}^2 \left|F_{p_2}\right|^2 \right) \left|F_q\right|^2 dxdy \right], \qquad q = s, i. \tag{21}$$

Finally, it is more common in third-order nonlinear media to use the nonlinear refractive n_2 in units m^2/W rather than $\chi^{(3)}$ in units m^2/V^2. It can be shown that $3\chi^{(3)} A_p^2 = 8\, n_2 I_p$ using the definitions of n_2 and $\chi^{(3)}$ [9], with I_p the intensity of a Fourier pump component p. Similarly, the factor $3\chi^{(3)} A_{p_1} A_{p_2}$ can be written as $8\, n_2 \sqrt{I_{p_1} I_{p_2}}$. Knowning the input pulse energy Q, I_p can be determined via $I_p = \frac{Q\tau\Delta\omega^2}{2\pi\sqrt{\pi}\, S_p} \, e^{-\tau^2 \left(\omega_p - \omega_{p_0}\right)^2}$.

3. Simulations

In this section, the developed model will be exploited in investigating photon-pair generation via SFWM parametric processes in periodically tapered waveguides (PTWs), in particular, dispersion-oscillating fibres and width-modulated silicon-nitride waveguides. The platforms are designed to operate in the normal-dispersion regime, where satisfying the phase-matching condition is usually hard to achieve in uniform single-mode waveguides. Operating in this regime will suppress unwanted nonlinear phenomena such as supercontinuum generation, soliton formation, or dispersive-wave emission that could ruin the aimed SFWM process under strong pumping [26]. To insure adiabatic propagation, only small modulation amplitude and relatively large tapering periods (in comparison to the operating wavelengths) have been explored [25]. The tapering period in the simulated structures has been discretised into 200 steps to increase the accuracy of the computational results.

3.1. Dispersion-oscillating fibres

These are silica solid-core sinusoidally tapered microstructured fibres made of a stack of hollow capillary tubes with a cross-sectional pitch σ, and a hole-diameter d [17]. The fibre pitch longitudinally varies as $\sigma(z) = \sigma_{\text{av}} \left[1 - \Delta\sigma \cos\left(2\pi z/\Lambda_{\text{T}}\right)\right]$, where σ_{av} is the average pitch, $\Delta\sigma$ is the modulation amplitude, and Λ_{T} is the tapering period. Figures 1(a) and 1(b) display the group index $n_g = c\beta_1$ (where β_1 is the first-order dispersion), and the second-order dispersion coefficient β_2 of a fibre with $\sigma_{\text{av}} = 1\ \mu$m, $\Delta\sigma = 0.1$, $d = 0.5\sigma$, and an output diameter 40σ. The fibre effective refractive indices used in these calculations have been computed via the empirical equations [27], including the material dispersion of silica [28]. Over the shown spectrum from 0.6 to 1 μm, the fibre dispersion is completely normal and the group index is gradually decrease with varying slopes.

Assuming a monochromatic pump source with a wavelength 780 nm and an input power 1 W, Fig. 1(c) shows the dependence of the mismatching between the propagation constants $\Delta\kappa$ of SFWM processes and the corresponding tapering period $\Lambda_{\text{T}} = 2\pi/\Delta\kappa$ on the signal wavelength

Optics EXPRESS

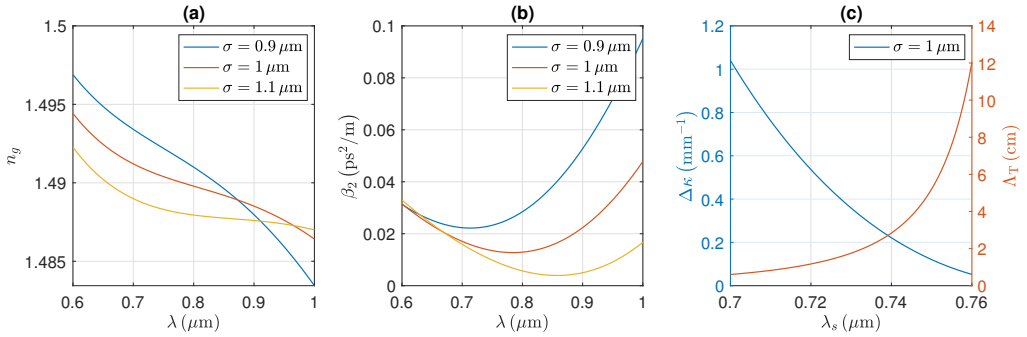

Fig. 1. (a,b) Wavelength-dependence of the group-index and second-order dispersion of a sinusoidally tapered microstructured fibres with a pitch σ varies between 0.9 and 1.1 μm, and a hole-diameter $d = 0.5\sigma$. (c) Dependence of the mismatching between the propagation constants $\Delta\kappa$ of a SFWM process and the tapering period Λ_T on the signal wavelength λ_s with a pump at 780 nm and an input power 1 W. The assumed fibre nonlinear refractive index is $n_2 = 2.25 \times 10^{-20}$ m^2/W. These parameters will be used in subsequent simulations, unless stated otherwise.

λ_s for the average pitch. These presented values of Λ_T are regarded as good estimates for the right ones needed to correct the phase-mismatching via the PTW-technique at a particular wavelength λ_s [19]. Close to the pump, Λ_T is in the few-centimetres range, which can be achievable using advanced post-treatment processes [17]. The PTW-technique can be used to generate photon-pairs, in principle, at any on-demand frequency. However, due to the current fabrication limitations, I will exploit this technique to demonstrate the ability to generate signal and idler photons at 750 and 812.5 nm. All interacting photons are in the fibre fundamental mode, and their transverse profiles are approximated as Gaussian distributions [9].

The right combinations between the modulation amplitude and tapering period that lead to an enhanced conversion efficiency of the expected number of photons $\langle\psi|\,\hat{N}\,(L,\omega_s)\,|\psi\rangle$ of a SFWM process at the targeted wavelengths are portrayed in Fig. 2(a) for the same number of periods M. The bright trajectories from left to right represent the 1st, 2nd,3rd,... -order tapering periods. The values of $\langle\hat{N}\rangle$ are normalised to the case when $\Delta\sigma = 0$, to quantify the enhancement using the PTW-technique. The expected number of signal photons are enhanced by 35 dB for only $M = 50$. The spatial growth of the single photons at a certain modulation amplitude is shown Fig. 2(b) for the 1st- and 2nd-order tapering periods (4.5 and 9 cm). The number of photons grows as an amplified oscillating function with single or double peaks within each cycle. Similar to periodically poled structures, higher rates are also obtained for shorter periods [3]. In addition, the value of the 2nd-order period (9 cm) slightly deviates from the exact one determined from Fig. 2(a), this results in accumulation of small phase mismatching during propagation that subsequently affects the growth rate.

The output spectrum of the photon pairs around the targeted wavelengths at the end of the fibre is depicted in Fig. 3(a) for a continuous pump wave at 780 nm. The spectrum is featured as a narrow sinc-function with very weak sidelobes that are significantly diminished for large number of periods. Figure 3(b) shows the 2D representation of the spectrum $\langle\hat{N}\rangle$ as a function of the signal λ_s and idler λ_i wavelengths. The pump wavelength at each point in this 2D plot is determined via satisfying the energy conservation $\omega_s + \omega_i = 2\omega_p$. This plot is the equivalent to the phase-matching function that shows how the wavelengths of the output single photons varies as the pump wavelength changes using the same nonlinear structure.

The whole spectra in the absence and presence of the waveguide modulation are displayed in

Optics EXPRESS

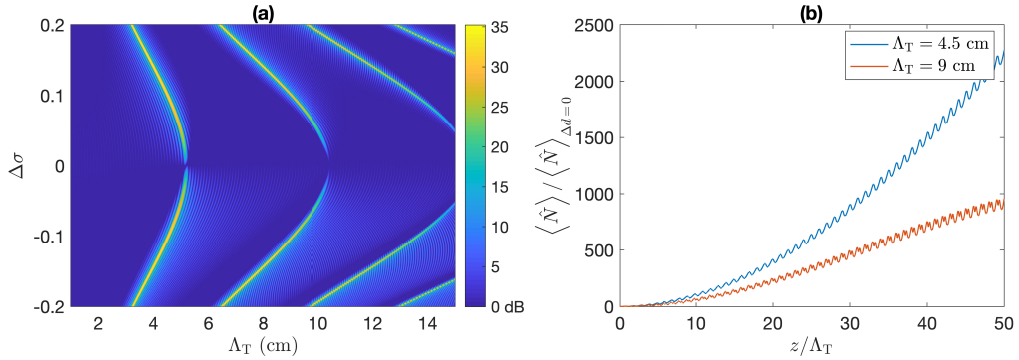

Fig. 2. (a) Dependence of $\langle\hat{N}\rangle$ of a SFWM process at a signal wavelength $\lambda_s = 750$ nm on the modulation amplitude $\Delta\sigma$ and tapering period Λ_T at the end of sinusoidally tapered fibres, for the same number of periods $M = 50$. (b) Spatial dependence of $\langle\hat{N}\rangle$ with $\Delta\sigma = 0.1$.

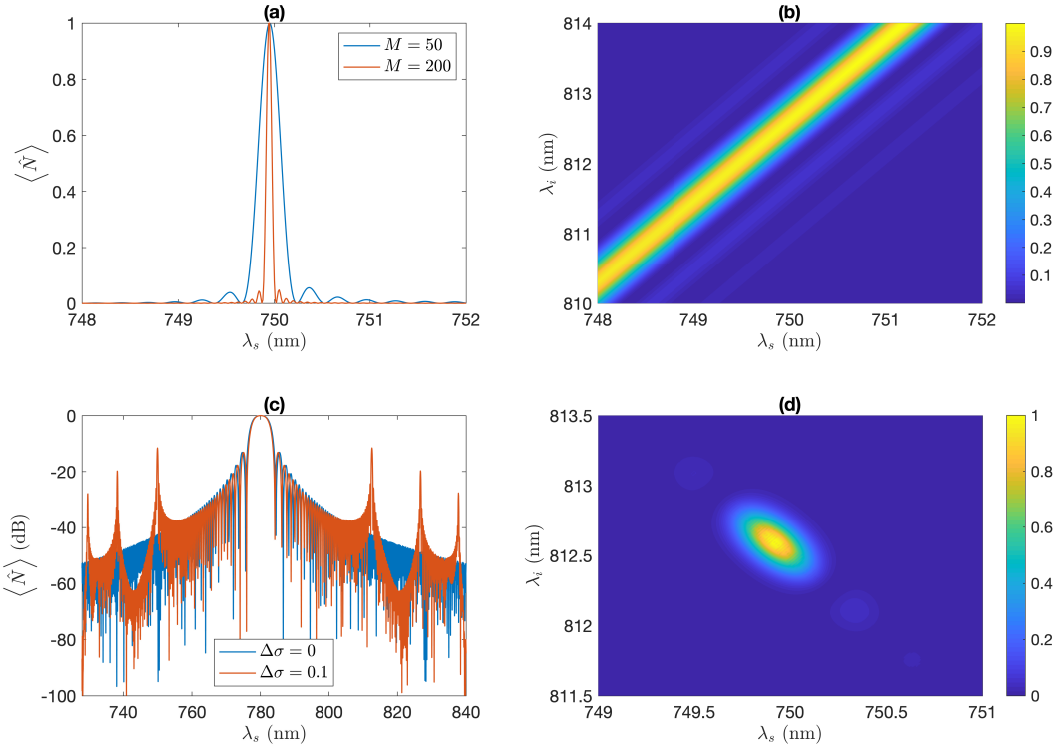

Fig. 3. (a,b) 1D and 2D spectral dependence of the expected number of photons $\langle\hat{N}\rangle$ generated in a modulated fibre with $\Delta\sigma = 0.1$ around the targeted wavelengths. (c) Dependence of $\langle\hat{N}\rangle$ on the signal wavelength over the entire spectrum. (d) Dependence of $\langle\hat{N}\rangle$ on the signal and idler wavelengths for a Gaussian pump with $Q = 1$ nJ and $\tau = 2.47$ ps. $M = 50$ and $\Lambda_T = 4.5$ cm in (b–d).

Optics EXPRESS

Fig. 3(c). This plot validates the developed quantum model, it resembles the output spectrum in the normal dispersion regime of fibre due to the classical nonlinear modulation instability effect. In a uniform waveguide with a normal dispersion, the propagation of a CW is stable against small perturbations [9]. However, this scenario is completely changed in a nonuniform waveguide, where modulation instability amplifies the background noise regardless the dispersion type. The frequencies of the amplified sidebands can be approximated with ≈ 3 nm difference from the simulations using the relation $\beta_2\Omega^2 + 2\gamma P = 2\pi l/\Lambda_T$, where $\Omega = \omega_s - \omega_p$ is the frequency shift from the pump source, β_2, and γ are the average second-order dispersion and nonlinear coefficient, P is the input power, and l is an integer [17]. The slight deviation is due to the negligence of the effect of the modulation amplitude in this equation.

Considering a Gaussian-pulse pump source with an input energy 1 nJ and a full-width-half-maximum 4 ps, the corresponding expected number of photons $\langle \hat{N} \rangle$ is portrayed in Fig. 3(d). This plot is the equivalent to the joint-spectral intensity distribution, which is usually obtained in the interaction Hamiltonian picture via tracking the evolution of the quantum biphoton state. Therefore, the 2D joint-spectral amplitude function $J(\omega_s, \omega_i)$ can be constructed in the introduced analysis in this paper via calculating the term $\mathbf{T}_{s,i}(1, 2)$ in the regime encompassses the targeted wavelengths of the signal and idler photons. This function J can be regarded as the the product between the phase-matching function and the pump-spectral envelope [29, 30].

The spectral-purity that measures the discorrelation between the output single photons is determined via the joint-spectral amplitude function. Using the singular-value decomposition J can be expressed as UVW, where U and W are unitary matrices represent the modes into which the initial quantum state has been decomposed, and V is a diagonal matrix describes how the modes in U and W are mixed together. Normalising V such that $\sum_i \rho_i^2 = 1$ with ρ_i its diagonal elements, the spectral purity is $\sum_i \rho_i^4$ [30]. To obtain a high spectral-purity the group-velocity-matching condition, in which group-velocity of the pump lies in between those of the signal and idler (as shown in Fig. 1(a)), needs to be satisfied [11]. The spectral purity in the case presented in Fig. 3(d) is 0.74 (taking into account the presence of the parasitic nonlinearities self- and cross-phase modulations). Having a shorter Gaussian pump source with width 1 ps the spectral purity increases to ≈ 0.93, which shows the ability of the PTW-technique in producing high-pure single photons at any desired frequencies.

3.2. Width-modulated silicon-nitride waveguides

A current key challenge in developing integrated single photons sources is isolating the pump photons from the converted single photons that are only within few nanometers spectral range [31]. The PTW-technique would provide a direct solution for this problem by enabling photon-pair generation at on-demand frequencies spectrally far from the pump. For this purpose, planar silicon-nitride waveguides, characterised by CMOS-compatibility, negligible two-photon absorption, and very weak Raman nonlinearity [22], have been also examined in this work. A sketch of the cross-sectional view of the planar waveguide used in the simulations is shown in Fig. 4(a). In this case, the core thickness h is fixed, while its width varies sinusoidally as $w(z) = w_{av}[1 - \Delta w \cos(2\pi z/\Lambda_T)]$ with w_{av} the average width and Δw the modulation. The fundamental TE mode of a wave at 1.064 μm in a waveguide with a core width $w = 1650$ nm and a thickness $h = 450$ nm is shown in Fig. 4(a). Simulations are performed using 'COMSOL', a commercial finite-element method, including the material dispersion of silica and silicon nitride. The dispersion of the waveguide is normal over the entire spectrum, as depicted in Fig. 4(b). The guiding loss is less than 0.1 dB/m for $\lambda < 1.4$ μm, then it rapidly increases to 3.8 dB/m at 1.6 μm.

Assuming a pump source with a central wavelength 1.064 μm and an input pump power 1 W, Fig. 4(c) shows the spectral dependence of the propagation-constant mismatching $\Delta\kappa$ of SFWM processes and the corresponding tapering periods for the average waveguide width. To generate photon-pairs with one photon in the telecommunication regime using this pump source, Λ_T in the

Optics EXPRESS

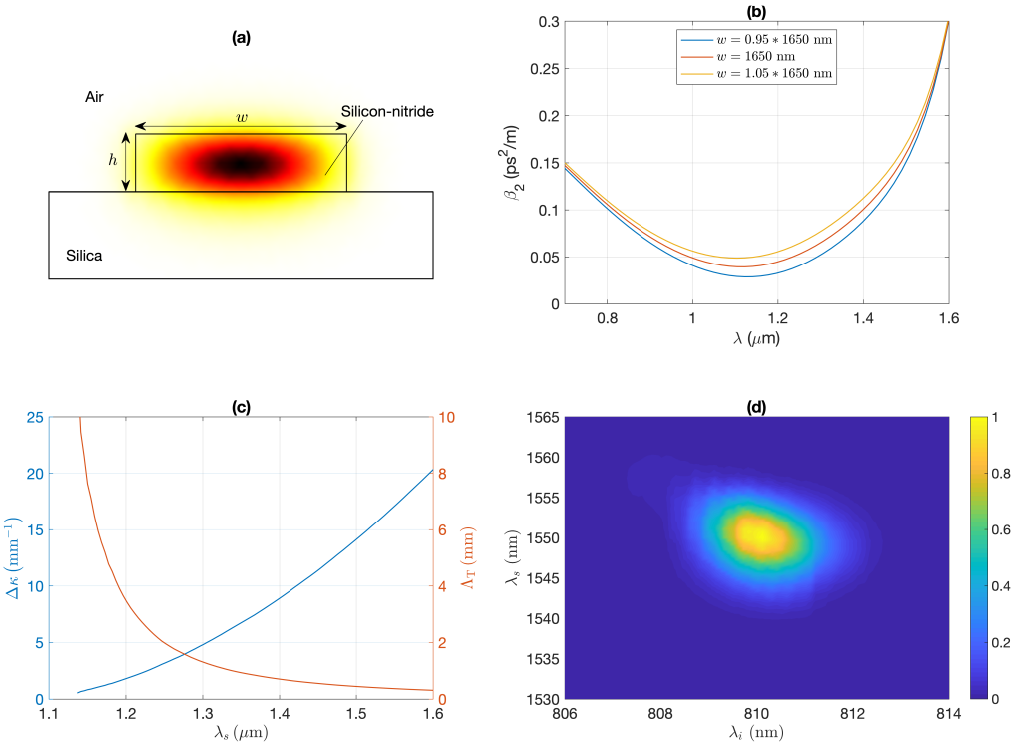

Fig. 4. A planar silicon-nitride PTW with w_{av} = 1650 nm, Δw = 0.05, h = 450 nm, Λ_T = 370 μm, M = 50, and $n_2 = 1.5 \times 10^{-18}$ m^2/W: (a) Fundamental TE mode at λ = 1064 nm and $w = w_{av}$. (b) Spectral-dependence of β_2 of the waveguide for different widths. (c) Dependence of $\Delta\kappa$ and the corresponding Λ_T on the signal wavelength λ_s at the average width, with a pump wavelength 1064 nm and an input power 1 W. (d) Dependence of $\langle \hat{N} \rangle$ on the signal and idler wavelengths for a Gaussian-pulse centred at 1064 nm with Q = 1 nJ and τ = 0.29 ps.

range of few-hundreds micrometers is needed, which is currently achievable [18]. The expected number of photons using a PTW of 50 periods under a Gaussian-pulse excitation is depicted in Fig. 4(d). The emission of photon-pairs at 810 and 1550 nm has been enhanced by 25 dB via the proper combination of the tapering period and modulation amplitude. The presented data has been smoothed to amend small irregularities, which might be due to the fact that an extremely fine mesh grid is required to precisely resolve the modes of this planar configuration especially at longer wavelengths. For the case displayed in Fig.4(d), the spectral purity is 0.82 ($\approx$ 0.9 with smoothing). In comparison, a spectral-purity of 0.87 has been recently obtained between photon pairs at 667 and 820 nm using a chip-based array of doped-silica waveguides and a pump source at 736 nm [1]. This shows the strong competitiveness of the proposed structure as an alternative pure highly efficient single-photon source with a widely tunable frequency range and CMOS-compatibility for integrated quantum applications.

4. Conclusions

In conclusion, I have developed a rigorous quantum model to study SFWM parametric processes in tapered waveguides for continuous and pulsed pump sources. The model calculates the

Optics EXPRESS

expected number photons of a certain spectral mode in the Heisenberg picture. The analysis precisely includes the effect of self- and cross-phase modulation on the SFWM processes, as well as material and waveguide dispersions, and the transverse profiles of the interacting modes. Both dispersion-oscillating fibres and width-modulated silicon-nitride waveguides, examples of PTWs, have been examined for enhancing photon-pairs generation at on-demand frequencies and with high spectral purities. The model results have been verified via retrieving the dynamics of the classical nonlinear modulation instability process in dispersion-oscillating fibres. In comparison to uniform waveguides, a 35 (25) dB enhancement in the expected number of photons can be achieved via a proper choice of the tapering period and modulation amplitude in microstructured fibres (planar waveguides) with only 50 periods. The output photons are characterised by having very narrow bandwidths, and relatively high spectral purities. The presented simulations theoretically validate the concept of the PTW-technique as a new efficient quasi-phase-matching scheme for photon-pair generation in third-order nonlinear materials, which will have a great leverage in the field of quantum and nonlinear optics. Finally, I anticipate that exploring non-periodic tapering patterns will be a fruitful future-research direction for optimising the spectral properties of the output photons.

Funding

Royal Society of Edinburgh (501100000332).

Acknowledgment

The author thanks F. Graffitti and Dr. A. Fedrizzi at Heriot-Watt University for useful discussions.

References

1. J. B. Spring, P. L. Mennea, B. J. Metcalf, P. C. Humphreys, J. C. Gates, H. L. Rogers, C. Söller, B. J. Smith, W. S. Kolthammer, P. G. R. Smith, and I. A. Walmsley, "Chip-based array of near-identical, pure, heralded single-photon sources," Optica **4**, 90–96 (2017).
2. J. A. Armstrong, N. Bloembergen, J. Ducuing, and P. S. Pershan, "Interactions between light waves in a nonlinear dielectric," Phys. Rev. **127**, 1918–1939 (1962).
3. M. M. Fejer, G. A. Magel, D. H. Jundt, and R. L. Byer, "Quasi-phase-matched second harmonic generation: tuning and tolerances," IEEE J. Quantum Electron. **28**, 2631–2654 (1992).
4. A. Eckstein, A. Christ, P. J. Mosley, and C. Silberhorn, "Highly efficient single-pass source of pulsed single-mode twin beams of light," Phys. Rev. Lett. **106**, 013603 (2011).
5. J. B. Spring, P. S. Salter, B. J. Metcalf, P. C. Humphreys, M. Moore, N. Thomas-Peter, M. Barbieri, X.-M. Jin, N. K. Langford, W. S. Kolthammer, M. J. Booth, and I. A. Walmsley, "On-chip low loss heralded source of pure single photons," Opt. Express **21**, 13522–13532 (2013).
6. F. Graffitti, P. Barrow, M. Proietti, D. Kundys, and A. Fedrizzi, "Independent high-purity photons created in domain-engineered crystals," Optica **5**, 514–517 (2018).
7. A. McMillan, J. Fulconis, M. Halder, C. Xiong, J. Rarity, and W. Wadsworth, "Narrowband high-fidelity all-fibre source of heralded single photons at 1570 nm," Opt. Express **17**, 6156–6165 (2009).
8. J. W. Silverstone, D. Bonneau, K. Ohira, N. Suzuki, H. Yoshida, N. Iizuka, M. Ezaki, C. M. Natarajan, M. G. Tanner, R. H. Hadfield, V. Zwiller, G. D. Marshall, J. G. Rarity, J. L. O'Brien, and M. G. Thompson, "On-chip quantum interference between silicon photon-pair sources," Nat. Photonics **8**, 104 (2013).
9. G. P. Agrawal, *Nonlinear Fiber Optics*, 4th ed. (Academic University, 2007).
10. J. G. Rarity, J. Fulconis, J. Duligall, W. J. Wadsworth, and P. S. J. Russell, "Photonic crystal fiber source of correlated photon pairs," Opt. Express **13**, 534–544 (2005).
11. K. Garay-Palmett, H. J. McGuinness, O. Cohen, J. S. Lundeen, R. Rangel-Rojo, A. B. U'Ren, M. G. Raymer, C. J. McKinstrie, S. Radic, and I. A. Walmsley, "Photon pair-state preparation with tailored spectral properties by spontaneous four-wave mixing in photonic-crystal fiber," Opt. Express **15**, 14870–14886 (2007).
12. Z. Vernon, M. Menotti, C. C. Tison, J. A. Steidle, M. L. Fanto, P. M. Thomas, S. F. Preble, A. M. Smith, P. M. Alsing, M. Liscidini, and J. E. Sipe, "Truly unentangled photon pairs without spectral filtering," Opt. Lett. **42**, 3638–3641 (2017).
13. P. Dong and A. G. Kirk, "Nonlinear frequency conversion in waveguide directional couplers," Phys. Rev. Lett. **93**, 133901 (2004).
14. R. J. A. Francis-Jones, T. A. Wright, A. V. Gorbach, and P. J. Mosley, "Engineered photon-pair generation by four-wave mixing in asymmetric coupled waveguides," arXiv:1809.10494 (2018).

Optics EXPRESS

15. J. B. Driscoll, N. Ophir, R. R. Grote, J. I. Dadap, N. C. Panoiu, K. Bergman, and R. M. Osgood, "Width-modulation of si photonic wires for quasi-phase-matching of four-wave-mixing: experimental and theoretical demonstration," Opt. Express **20**, 9227–9242 (2012).
16. A. Armaroli and F. Biancalana, "Tunable modulational instability sidebands via parametric resonance in periodically tapered optical fibers," Opt. Express **20**, 25096–25110 (2012).
17. A. Mussot, M. Conforti, S. Trillo, F. Copie, and A. Kudlinski, "Modulation instability in dispersion oscillating fibers," Adv. Opt. Photon. **10**, 1–42 (2018).
18. D. D. Hickstein, G. C. Kerber, D. R. Carlson, L. Chang, D. Westly, K. Srinivasan, A. Kowligy, J. E. Bowers, S. A. Diddams, and S. B. Papp, "Quasi-phase-matched supercontinuum generation in photonic waveguides," Phys. Rev. Lett. **120**, 053903 (2018).
19. M. F. Saleh, "Quasi-phase-matched $\chi^{(3)}$-parametric interactions in sinusoidally tapered waveguides," Phys. Rev. A **97**, 013850 (2018).
20. B. Huttner, S. Serulnik, and Y. Ben-Aryeh, "Quantum analysis of light propagation in a parametric amplifier," Phys. Rev. A **42**, 5594–5600 (1990).
21. O. Alibart, J. Fulconis, G. K. L. Wong, S. G. Murdoch, W. J. Wadsworth, and J. G. Rarity, "Photon pair generation using four-wave mixing in a microstructured fibre: theory versus experiment," New J. Phys. **8**, 67 (2006).
22. H. Guo, C. Herkommer, A. Billat, D. Grassani, C. Zhang, M. H. P. Pfeiffer, W. Weng, C.-S. Brès, and T. J. Kippenberg, "Mid-infrared frequency comb via coherent dispersive wave generation in silicon nitride nanophotonic waveguides," Nat. Photonics **12**, 330–335 (2018).
23. M. F. Saleh, W. Chang, P. Hölzer, A. Nazarkin, J. C. Travers, N. Y. Joly, P. S. J. Russell, and F. Biancalana, "Theory of photoionization-induced blueshift of ultrashort solitons in gas-filled hollow-core photonic crystal fibers," Phys. Rev. Lett. **107**, 203902 (2011).
24. Y. R. Shen, "Quantum statistics of nonlinear optics," Phys. Rev. **155**, 921–931 (1967).
25. J. D. Love, W. M. Henry, W. J. Stewart, R. J. Black, S. Lacroix, and F. Gonthier, "Tapered single-mode fibres and devices. i. adiabaticity criteria," Optoelectronics IEEE Proc. J. **138**, 343–354 (1991).
26. A. S. Kowligy, D. D. Hickstein, A. Lind, D. R. Carlson, H. Timmers, N. Nader, D. L. Maser, D. Westly, K. Srinivasan, S. B. Papp, and S. A. Diddams, "Tunable mid-infrared generation via wide-band four-wave mixing in silicon nitride waveguides," Opt. Lett. **43**, 4220–4223 (2018).
27. K. Saitoh and M. Koshiba, "Empirical relations for simple design of photonic crystal fibers," Opt. Express **13**, 267–274 (2005).
28. B. E. A. Saleh and M. C. Teich, *Fundamentals of Photonics*, 2nd ed. (Wiley, 2007).
29. A. Dosseva, L. Cincio, and A. M. Brańczyk, "Shaping the joint spectrum of down-converted photons through optimized custom poling," Phys. Rev. A **93**, 013801 (2016).
30. P. J. Mosley, J. S. Lundeen, B. J. Smith, and I. A. Walmsley, "Conditional preparation of single photons using parametric downconversion: a recipe for purity," New J. Phys. **10**, 093011 (2008).
31. L. Pavesi and D. J. Lockwood, *Silicon Photonics III* (Springer-Verlag, 2016).